

A large fraction of hydrogen-rich supernova progenitors experience elevated mass loss shortly prior to explosion

RACHEL J. BRUCH,¹ AVISHAY GAL-YAM,¹ STEVE SCHULZE,¹ OFER YARON,¹ YI YANG,¹ MAAYANE SOUMAGNAC,^{1,2}
 MICKAEL RIGAULT,³ NORA L. STROTJOHANN,¹ ERAN OFEK,¹ JESPER SOLLERMAN,⁴ FRANK J. MASCI,⁵
 CRISTINA BARBARINO,⁴ ANNA Y. Q. HO,⁶ CHRISTOFFER FREMLING,⁶ DANIEL PERLEY,⁷ JAKOB NORDIN,⁸
 S. BRADLEY CENKO,^{9,10} S. ADAMS,⁶ IGOR ADREONI,⁶ ERIC C. BELLM,¹¹ NADIA BLAGORODNOVA,¹² MATTIA BULLA,⁴
 KEVIN BURDGE,⁶ KISHALAY DE,⁶ SUHAIL DHAWAN,⁴ ANDREW J. DRAKE,¹³ DMITRY A. DUEV,¹³ ALISON DUGAS,¹⁴
 MATTHEW GRAHAM,⁶ MELISSA L. GRAHAM,¹⁵ JACOB JENCSON,⁶ EMIR KARAMEHMETOGLU,^{4,16} MANSI KASLIWAL,⁶
 YOUNG-LO KIM,³ SHRINIVAS KULKARNI,⁶ THOMAS KUPFER,¹⁷ ASHISH MAHABAL,¹⁸ A. A. MILLER,^{19,20}
 THOMAS A. PRINCE,¹³ REED RIDDLE,²¹ Y. SHARMA,⁶ ROGER SMITH,²¹ FRANCESCO TADDIA,^{4,16} KIRSTY TAGGART,⁷
 RICHARD WALTERS,²² AND LIN YAN⁶

¹Department of Particle Physics and Astrophysics Weizmann Institute of Science 234 Herzl St. 76100 Rehovot, Israel

²Computational Cosmology Center, Lawrence Berkeley National Laboratory, 1 Cyclotron Road, Berkeley, CA 94720, USA

³Université de Lyon, Université Claude Bernard Lyon 1, CNRS/IN2P3, IP2I Lyon, F-69622, Villeurbanne, France

⁴The Oskar Klein Centre, Department of Astronomy, Stockholm University, AlbaNova, SE-106 91 Stockholm, Sweden

⁵IPAC, California Institute of Technology, 1200 E. California Blvd, Pasadena, CA 91125, USA

⁶Cahill Center for Astrophysics, California Institute of Technology, MC 249-17, 1200 E California Boulevard, Pasadena, CA, 91125, USA

⁷Astrophysics Research Institute, Liverpool John Moores University, Liverpool Science Park, 146 Brownlow Hill, Liverpool L3 5RF, UK

⁸Institute of Physics, Humboldt-Universität zu Berlin, Newtonstr. 15, 12489 Berlin, Germany

⁹Astrophysics Science Division, NASA Goddard Space Flight Center, MC 661, Greenbelt, MD 20771, USA

¹⁰Joint Space-Science Institute, University of Maryland, College Park, MD 20742, USA

¹¹DIRAC Institute, Department of Astronomy, University of Washington, 3910 15th Avenue NE, Seattle, WA 98195, USA

¹²Department of Astrophysics/IMAPP, Radboud University, Nijmegen, The Netherlands

¹³Division of Physics, Mathematics and Astronomy, California Institute of Technology, Pasadena, CA 91125, USA

¹⁴Department of Physics and Astronomy, Watanabe 416, 2505 Correa Road, Honolulu, HI 96822

¹⁵University of Washington, Department of Astronomy Box 351580 Seattle WA 98195-1580, USA

¹⁶Department of Physics and Astronomy, Aarhus University, Ny Munkegade 120, DK-8000 Aarhus C, Denmark

¹⁷Kavli Institute for Theoretical Physics, University of California, Santa Barbara, CA 93106, USA

¹⁸Division of Physics, Mathematics, and Astronomy, California Institute of Technology, Pasadena, CA 91125, USA

¹⁹Center for Interdisciplinary Exploration and Research in Astrophysics and Department of Physics and Astronomy, Northwestern University, 1800 Sherman Ave, Evanston, IL 60201, USA

²⁰The Adler Planetarium, Chicago, IL 60605, USA

²¹Caltech Optical Observatories, California Institute of Technology, Pasadena, CA 91125, USA

²²Caltech Optical Observatories, California Institute of Technology, MC 249-17, 1200 E California Boulevard, Pasadena, CA, 91125

Submitted to ApJ

ABSTRACT

Spectroscopic detection of narrow emission lines traces the presence of circumstellar mass distributions around massive stars exploding as core-collapse supernovae. Transient emission lines disappearing shortly after the supernova explosion suggest that the spatial extent of such material is compact, and hence imply an increased mass loss shortly prior to explosion. Here, we present a systematic survey for such transient emission lines (Flash Spectroscopy) among Type II supernovae detected in the first year of the Zwicky Transient Facility (ZTF) survey. We find that at least six out of ten events for which a spectrum was obtained within two days of estimated explosion time show evidence for such transient flash lines. Our measured flash event fraction ($> 30\%$ at 95% confidence level) indicates that elevated mass loss is a common process occurring in massive stars that are about to explode as supernovae.

Keywords: supernova:general - methods: observational - stars: mass-loss - stars: massive

1. INTRODUCTION

Massive stars ($M > 8 M_{\odot}$) explode as core-collapse supernovae (CC SNe; Smartt 2015; Gal-Yam 2017). Such massive stars often experience mass loss from their outer layers, due to stellar winds, binary interaction, or eruptive mass-loss events (see, e.g., Smith 2014 and references within). The mass lost by these stars forms distributions of circumstellar medium (CSM). The properties of the CSM depend on the mass-loss rate, the velocity of the flow, and the duration of the process.

When a massive star surrounded by CSM explodes as a CC SN, signatures of the CSM may manifest as spectroscopic features with a narrow width reflecting the mass-loss velocity, that is typically low compared to the expansion velocity of the supernova ejecta. In Type IIn SNe (e.g., Schlegel 1990, Filippenko 1997, Gal-Yam 2017, Kiewe et al. 2012, Taddia et al. 2013, Nyholm et al. 2019) narrow hydrogen lines persist for weeks to years after explosion, indicating an extensive CSM distribution. Type Ibn events (e.g., Pastorello et al. 2016, Gal-Yam 2017, Hosseinzadeh et al. 2015, Karamehmetoglu et al. 2019) show strong emission lines of helium, suggesting recent mass loss from stripped progenitors. In both Types IIn and Ibn, there is evidence that in at least some cases, the mass-loss is generated by precursor events, prior to the SN explosion (e.g. Pastorello et al. 2007, Foley et al. 2007, Ofek et al. 2014, Strotjohann et al., in prep.)

If the extension of the CSM is confined to a relatively compact location around an exploding star or if its density is low, the explosion shock-breakout flash may ionize the CSM. The resulting recombination emission lines will be transient, persisting only until the SN ejecta overtake and engulf the denser parts of the CSM (supernovae with “flash ionized” emission lines; Gal-Yam et al. 2014). Such events later evolve spectroscopically in a regular manner, e.g., presenting photospheric spectra with broad P-Cygni line profiles.

Several serendipitous observation of such “flash features” in early supernova spectra were made over the years (e.g., Niemela et al. 1985, Garnavich & Ann 1994, Quimby et al. 2007). We define flash features here as transient narrow emission lines (of the order of $\approx 10^2$ km s $^{-1}$) of highly ionised species (e.g.: He II, C III, N III, N IV) in the early phases of the supernova event (less than a week, in general from estimated explosion). Gal-Yam et al. (2014) presented very early observations of the Type I Ib SN 2013cu, and noted that such flash features could be routinely observed by modern high-

cadence SN surveys and probe the composition of the pre-explosion mass loss, and hence the surface composition of the progenitor star, which is hard to measure by other means. This motivated additional work on such flash objects. For example, Yaron et al. (2017) presented a time-series of early spectra and used it to constrain the CSM distribution around the spectroscopically normal SN 2013fs, showing that the CSM was lost from the progenitor in the year prior to its explosion. Hosseinzadeh et al. (2018) studied the low-luminosity Type II event SN 2016bkv which showed early flash ionisation features. They suggest that its early light-curve bump could suggest a contribution from CSM interaction to the early light curve, motivating the systematic study of early light curves of Type II SNe showing flash features to distinguish between properties originating from the CSM (e.g., perhaps, peak luminosity) and those determined by the progenitors via shock cooling emission. Several theoretical investigations also focused on such events (e.g., Groh 2014, Dessart et al. 2017, Moriya et al. 2017 and Boian & Groh 2020).

A systematic study of such transient signatures of CSM around SN II progenitor stars has been limited by the challenge of routinely observing CC SNe early enough (typically within less than a few days from explosion), before these features disappear. Khazov et al. (2016) conducted the first study of the occurrence of flash ionisation in Type II SNe using data from the PTF and iPTF surveys, and gathered 12 objects showing flash ionisation features. They estimate that more than $\sim 20\%$ of SNe II show flash ionisation features, but their analysis is limited by the heterogeneity of their data.

Routine and systematic observations of young (“infant”) SNe was one of the main goals of the ZTF survey (Gal-Yam 2019; Graham et al. 2019). Here, we present our systematic search and follow-up observations of infant Type II SNe from ZTF. We use a sample of 28 events collected during the first year of ZTF operation, ten of which were spectroscopically observed within two days of estimated explosion, to place a lower limit on the fraction of SN progenitor stars embedded in CSM.

In section § 2, we describe the properties of our infant SN survey and the construction of our sample of SNe II. In § 3 we present our analysis, in § 4 we discuss our findings, and we conclude in § 5.

2. OBSERVATIONS AND SAMPLE CONSTRUCTION

2.1. Selecting infant SNe from the ZTF partnership stream

The Zwicky Transient Facility (ZTF) is a wide-field, high cadence, multiband survey that started operating in March 2018 (Bellm et al. 2019; Graham et al. 2019). ZTF imaging is obtained using the Samuel Oschin 48” Schmidt telescope at Palomar observatory (P48). ZTF observing time is divided among three programs: the public (MSIP) 3-day all-sky survey, partnership surveys, and Caltech programs. This paper is based on data obtained by the high-cadence partnership survey. As part of this program, during 2018, extra-galactic survey fields were observed in both the ZTF g- and r-bands 2-3 times per night per band. New images were processed through the ZTF pipeline (Masci et al. 2019) and reference images built by combining stacks of previous ZTF imaging in each band were then subtracted using the Zackay et al. (2016) image subtraction algorithm (ZOGY). A 30s integration time was used in both *g*- and *r*-band exposures, and a 5σ detection limit down to ~ 20.5 mag in *r* can be reached in a single observation.

We conducted our year-1 ZTF survey for infant SNe following the methodology of Gal-Yam et al. (2011). We selected potential targets via a custom filter running on the ZTF alert stream using the GROWTH Marshal platform (Kasliwal et al. 2019). The filter scheme was based on the criteria listed in Table 1.

Alerts that passed our filter (typically 50 – 100 alerts per day) were then visually scanned by a duty astronomer, in order to reject various artefacts (such as unmasked bad pixels or ghosts) and false positive signals, such as flaring M stars, CVs and AGN. Most spurious sources could be identified by cross matching with additional catalogues (e.g., *WISE* IR photometry (Wright et al. 2010) to detect red M stars, the Gaia DR2 catalog (Gaia Collaboration et al. 2018), and catalogs from time domain surveys such as the Palomar Transient Factory (PTF; Law et al. 2009) and the Catalina Real-Time Survey (CRTS; Drake et al. 2014) for previous variability of CVs and AGN.

Due to time-zone differences, our scanning team (located mostly at the Weizmann Institute in Israel and at the Oskar Klein Center (OKC) in Sweden) could routinely scan the incoming alert stream during the California night time, with the goal of triggering spectroscopic follow-up of promising infant SN candidates within hours of discovery (and thus typically within < 2 days from explosion), as well as *Swift* (Gehrels et al.

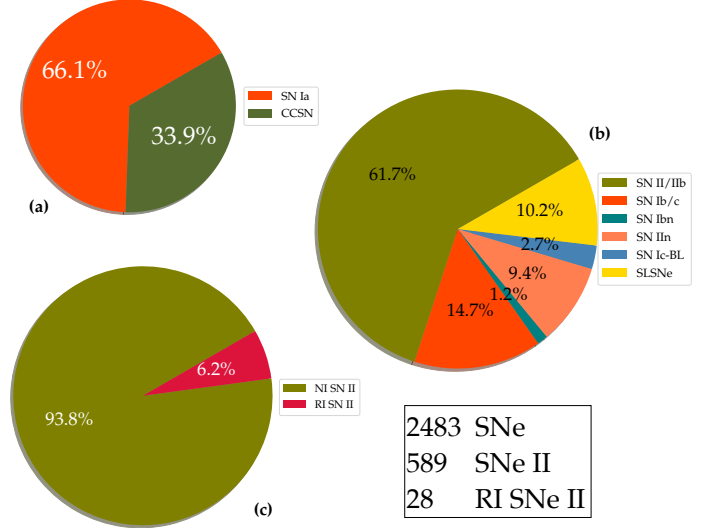


Figure 1. ZTF Spectroscopically-confirmed SN discovery statistics during 2018. (a) Most events (63%) are SNe Ia; CC SNe comprise about 37%. (b) The division among CC SN sub-classes (c) The fraction of real infant (RI) SNe II is 4.8% of the total Type II population. NI stands for the Non Infant SN II population (see text).

2004) Target-of-Opportunity (ToO) UV photometry.

2.2. Sample Construction

Figure 1 shows the SN Type distribution amongst the ~ 2500 spectroscopically-confirmed SNe gathered by ZTF between March and December 2018. About 37% are core-collapse events, and $\sim 63\%$ of those are of Type II. Since the large majority of flash events are SNe II, we can only place statistically meaningful constraints on the frequency of this phenomenon among Type II SNe. We therefore analyze here this population only.

Our infant SN program allowed us to obtain early photometric and spectroscopic follow-up of young SNe. However, it is possible that we have missed some relevant candidates. In order to ensure the completeness of our sample, we therefore inspected all spectroscopically classified SNe II (including subtypes IIn and I Ib) from ZTF¹ using the ZTFquery package (Rigault 2018). We pulled from this sample all events (the large majority) lacking a ZTF non-detection limit within 2.5 days prior to the first detection recorded on the ZTF Marshal. To include events in our final sample, we required that they show significant and rapid increase in flux, as previously observed for very young SNe (e.g., Gal-Yam et al. 2014, Yaron et al. 2017), with respect to the last

¹ between March 2018 and December 2018

Table 1. Filter criteria selecting infant SN candidates

<i>Stationary</i>	Reject solar-system objects using apparent motion
<i>Recent limit</i>	Require a non-detection limit within < 2.5 days from the first detection
<i>Extragalactic</i>	Reject alerts within 14 degrees from the Galactic plane
<i>Significant</i>	Require a ZOGY score of > 5
<i>Stellar</i>	Require a SG (star-galaxy) score of > 0.49

non-detection. This excludes older events that are just slightly below our detection limit and are picked up by the filter when they slowly rise, or when conditions improve. We implemented a cut on the observed rise of Δr or $\Delta g > 0.5$ mag with respect to the recent limit in the same band, and note all events that satisfy this cut as “real infant” (RI; Fig. 1, panel C).

All in all, we gathered 43 candidates which fulfilled the RI criteria. Additional inspection led us to determine that 15 candidates were spurious (see Appendix A for details). Our final sample (Table 2) thus includes a total of 28 RI Type II SNe, or about 5% of all the SNe II found by the ZTF survey for 2018. During its first year of operation (starting March 2018), ZTF obtained useful observations for our program during approximately 32 weeks, excluding periods of reference image building (initially), periods dedicated to Galactic observations, and periods of technical/weather closure. We therefore find that the survey provided about one real infant SN II per week.

2.3. Spectroscopic Observations

Our goal was to obtain rapid spectroscopy of RI SN candidates following the methods of Gal-Yam et al. (2011). This was made possible using rapid ToO follow-up programs as well as on-request access to scheduled nights on various telescopes. During the scanning campaign, we applied the following criteria for rapid spectroscopic triggers. The robotic SEDm (see below) was triggered for all candidates brighter than a threshold limiting magnitude (19 mag during 2018). Higher resolution spectra (using WHT, Gemini or other available instruments) were triggered for events showing recent non-detection limits (within 2.5 d prior to first detection) as well as a significant rise in magnitude compared to a recent limit or within the observing night.

P60/SEDm—The Spectral Energy Distribution Machine (SEDm; Ben-Ami et al. 2012; Blagorodnova et al. 2018; Neill 2019) is a high-throughput, low-resolution spectrograph, mounted on the 60” robotic telescope (P60; Cenko et al. 2006) at Palomar observatory. 65% of the time on the SEDm was dedicated to ZTF partnership follow up. SEDm data are reduced using an automated pipeline (Rigault et al. 2019). The co-location of the P60 and ZTF/P48 on the same mountain, as

well as the P60 robotic response capability, enable very short (often same-night) response to ZTF events, sometimes very close to the time of first detection (e.g., see ZTF18abwlsoi, below). However, the low resolution ($R \sim 100$) of the instrument limits our capability to characterise narrow emission lines. This, along with the overall sensitivity of the system, motivated us to try to obtain higher-resolution follow-up spectroscopy with other, larger, telescopes, in particular for all infant SNe detected below a magnitude cut of $r \sim 19$ mag.

P200/DBSP—We used the Double Beam SPectrograph (DBSP; Oke & Gunn 1982) mounted on the 5m Hale telescope at Palomar Observatory (P200) to obtain follow-up spectroscopy in either ToO mode or during classically scheduled nights. The default configuration used the 600/4000 grism on the blue side, the 316/7150 grating on the red side, along with the D55 dichroic, achieving a spectral resolution $R \sim 1000$. Spectra obtained with DBSP were reduced using the pyraf-dbsp pipeline (Bellm & Sesar 2016).

WHT-ISIS/ACAM—We obtained access to the 4.2m William Herschel Telescope (WHT) at the Observatorio del Roque de los Muchachos in La Palma, Spain via the Optical Infrared Coordination Network for Astronomy (OPTICON²) program³. We used both single-slit spectrographs ISIS and ACAM (Benn et al. 2008) in ToO service observing mode. The delivered resolutions were $R \sim 1000$ and $R \sim 400$, respectively. Spectral data were reduced using standard routines within IRAF⁴.

Keck/LRIS—We used the Low-Resolution Imaging Spectrometer (LRIS; Oke et al. 1995) mounted on the Keck-I 10m telescope at the W. M. Keck Observatory in Hawaii in either ToO mode or during scheduled nights. The data were reduced using the LRIS automated reduction pipeline Lpipe (Perley 2019).

² <https://www.astro-opticon.org/index.html>

³ Program IDs OPT/2017B/053, OPT/2018B/011, OPT/2019A/024, PI Gal-Yam

⁴ IRAF is distributed by the National Optical Astronomy Observatories, which are operated by the Association of Universities for Research in Astronomy, Inc., under cooperative agreement with the National Science Foundation.

GMOS/Gemini—We used the Gemini Multi-Object Spectrographs (GMOS; Hook et al. 2004) mounted on the Gemini North 8m telescope at the Gemini Observatory on Mauna Kea, Hawaii. All observations were conducted at small airmass ($\lesssim 1.2$). For each SN, we obtained 2×900 s exposures using the B600 grating with central wavelengths of 520 nm and 525 nm. The 5 nm shift in the effective central wavelength was applied to cover the chip gap, yielding a total integration time of 3600 s. A $1.0''$ -wide slit was placed on each target at the parallactic angle. The GMOS data were reduced following standard procedures using the Gemini IRAF package.

APO/DIS—We used the Dual Imaging Spectrograph (DIS) on the Astrophysical Research Consortium (ARC) 3.5 m telescope at Apache Point Observatory (APO) during scheduled nights. The data were reduced using standard procedures and calibrated to a standard star obtained on the same night using the PyDIS package (Davenport 2018).

All the data presented in this paper will be made public on WISEREP (Yaron & Gal-Yam 2012).

2.4. Photometry

The ZTF alert system (Patterson et al. 2018) provides on the fly photometry (Masci et al. 2019) and astrometry based on a single image for each alert. In order to improve our photometric measurements (and in particular, to test the validity of non-detections just prior to discovery) we performed forced PSF photometry at the location of each event. As shown by Yaron et al. (2019), the 95% astrometric scatter among ZTF alerts is $\sim 0.44''$; for our events we have multiple detections, with typically higher signal-to-noise ratio data around the SN peak compared to the initial first detections. We therefore compute the median coordinates of all the alert packages and perform forced photometry using this improved astrometric location.

We use the pipeline developed by F. Masci and R. Laher⁵ to perform forced PSF photometry at the median SN centroid on the ZTF difference images available from the IRSA database. For each light curve, we filter out measurements returned by the pipeline with non-valid flux values.

We perform a further quality cut on each light curve by rejecting observations with a data quality parameter *scisigpix*⁶ that is more than 5 times the median absolute

deviation (MAD) away from the median of this parameter for each light curve. We also remove faulty measurements where the *infobitssci* parameter is not zero. According to the Masci & Laher prescription we rescale the flux errors by the square root of the χ^2 of the PSF fit estimate in each image. We then correct each measured forced photometry flux value by the photometric zero point of each image, as provided by the pipeline:

$$f_{zp,corrected} = f_{forced-phot} \times 10^{-0.4 \times z_p} \quad (1)$$

We determine our zero-flux baseline using forced photometry observations obtained prior to the SN explosion. We calculate the median of these observations, reject outliers that are > 3 MAD away from the median, re-calculate the median and subtract it from our measured post-explosion flux values; these corrections are typically very small, of the order of $< 0.1\%$ of the supernova flux values.

If the ratio between the measured flux and the uncertainty σ is below 3, we consider this measurement as a non-detection, and report a 5σ upper limit. Otherwise (if the flux to error ratio is above 3σ) we report the flux, magnitude and respective errors. Finally, we correct for Galactic extinction using the python package *extinction*⁷, using local extinction values from Schlafly & Finkbeiner (2011) and assuming a selective extinction of $R_V = 3.1$ and the Cardelli et al. (1989) extinction law. We also correct the light curves to restframe time according to the spectroscopic redshifts.

We recovered detections prior to the first detection by the real-time pipeline using the forced photometry pipeline in 11 cases⁸. We redefined the first detection and last non-detection according to the forced photometry pipeline measurements in these cases.

We present our photometry for all RI objects in Table 3.

3. ANALYSIS AND RESULTS

In this section, we study the 28 RI SNe that passed our selection criteria, excluding spurious candidates (see Appendix A for details). In order to measure the fraction of objects showing flash features and thus evidence for CSM, we estimate the explosion time based on ZTF forced photometry light curves. We then define subsamples based on the SN age (relative to estimated explosion) at the time the first spectrum was obtained.

⁷ <https://github.com/kbarbary/extinction>

⁸ ZTF18aarqxbw, ZTF18aavpady, ZTF18aawyjjq, ZTF18abcezmh, ZTF18abckutn, ZTF18abcptmt, ZTF18abdbysy, ZTF18abddjpt, ZTF18abokyfk, ZTF18abrljc, ZTF18abvvmdf

⁵ <http://web.ipac.caltech.edu/staff/fmasci/ztf/forcedphot.pdf>

⁶ A parameter calculated by the pipeline that measures the pixel noise in each science image

Table 2. Sample of Real Infant 2018 (28 objects)

IAU name (SN)	Internal ZTF name	Type ^a name	Redshift z	Explosion JD Date	Error [d]	First detection [d] ^b	Last non detection [d]	First spectrum [d]	Telescope/ instrument	Flash
2018grf	18abwlsoi	SN II [19]	0.050	2458377.6103	0.0139	0.0227	-0.8725	0.1407	P60/SEDm	✓
2018fnz	18abojpnrr	SN IIb [30]	0.037	2458351.7068	0.0103	0.0102	-0.0103	0.1902	P60/SEDm	✗
2018dfi	18abffyqp	SN IIb [44]	0.031	2458307.2540	0.4320	0.4320	-0.4320	0.6180	P200/DBSP	✓
2018cxn	18abckutn	SN II [26]	0.040	2458289.8074	0.4189	0.0576	-0.0494	0.9406	P200/DBSP	✗
2018dfc	18abeajml	SN II [27]	0.037	2458303.7777	0.0118	0.0213	-0.9806	1.0153	P60/SEDm	✓
2018fif	18abokyfk	SN II [37]	0.017	2458350.9535	0.3743	-0.0635	-1.0525	1.0525	P200/DBSP	✓
2018gts	18abvvmdf	SN II [20]	0.030	2458375.1028	0.5551	-0.4688	-1.3648	1.5162	P60/SEDm	✓
2018cyg	18abdbysy	SN II [28]	0.011	2458294.7273	0.2034	0.0297	0.0147	1.6727	WHT/ACAM	?
2018cug	18abcptmt	SN II [29]	0.050	2458290.9160	0.0250	-0.0066	-0.0670	1.7960	P60/SEDm	✓
2018egh	18abgqvwv	SN II [10]	0.038	2458312.7454	0.4351	0.9846	0.0931	1.8236	WHT/ISIS	?
2018bqs	18aarpttw	SN II [10]	0.047	2458246.8133	0.0071	0.0087	-0.9926	2.0867	APO/DIS	✗
2018fsm	18absldfl	SN II [21]	0.040	2458363.4226	0.4565	0.4564	-0.4564	2.3674	P60/SEDm	✗
2018bge	18aaqkoyr	SN II [67]	0.023	2458243.1671	0.5180	0.5179	-0.5180	2.5169	P200/DBSP	✗
2018leh	18adbmrug	SN II In [16]	0.024	2458481.7505	0.9485	0.9485	-0.9485	3.6985	WHT/ISIS	✓
2018iua	18acploez	SN II [10]	0.040	2458439.9877	0.9784	0.9783	-0.9783	3.7933	P60/SEDm	✗
2018gvn	18abyvenk	SN II [22]	0.040	2458385.6198	0.0011	0.0012	-0.8565	6.1122	P60/SEDm	✗
2018clq	18aatlfus	SN II [31]	0.045	2458248.8967	0.9564	0.9564	-0.9564	6.9274	P60/SEDm	✗
2018ccp	18aawyjjq	SN II [25]	0.040	2458263.7743	0.1241	0.0106	-0.8684	8.1087	P60/SEDm	✗
2018lth	18ayayxxew	SN II [10]	0.061	2458278.6531	0.9154	0.0509	-1.9102	8.1589	Keck/LRIS	✗
2018inm	18achtnvk	SN II [23]	0.040	2458432.9113	0.6895	1.9927	1.9497	9.0137	P60/SEDm	✗
2018iwe	18abufaej	SN II [10]	0.062	2458368.8561	0.0179	0.0179	-0.0179	12.0159	P60/SEDm	✗
2018fso	18abrljlc	SN II [32]	0.050	2458357.6987	0.8255	-0.0177	-0.9157	14.0113	P60/SEDm	✗
2018efd	18abgrbjb	SN IIb [33]	0.030	2458312.8922	0.3938	0.8568	0.8244	14.9388	P60/SEDm	✗
2018cyh	18abcezmh	SN II [10]	0.057	2458286.3752	0.6050	0.4348	0.3898	16.5678	P60/SEDm	✗
2018ltg	18aarqxbw	SN II [10]	0.048	2458241.4360	3.4950	3.4950	-3.4950	37.5310	P200/DBSP	✗
2018lti	18abddjpt	SN II [10]	0.070	2458294.6217	0.1224	0.1693	-0.7917	40.2333	P60/SEDm	✗
2018efj	18abimhf	SN II [24]	0.050	2458320.6574	0.0210	0.0096	-0.9028	42.0096	P60/SEDm	✗
2018cfj	18aavpady	SN II [10]	0.047	2458256.4531	0.4771	0.4771	-0.4771	55.0469	Keck/LRIS	✗

^aClassification reports referenced in square brackets^bAll times reported relative to the estimated explosion date in fractional days

3.1. Explosion time estimation

In order to estimate the explosion time, which we define here as the time of zero-flux, we fit a general power law of the form to our flux measurements:

$$f(t) = a \times (t - t_{exp})^n \quad (2)$$

using the routine `curvefit` within the *astropy* python package (Astropy Collaboration et al. 2013). We fit the first 2 days of data following the first detection as well as the first 5 days (see Fig. 2 for example) in both the *g* and *r*-bands. The estimated explosion time is taken as the weighted mean of the four fits, and we adopt the standard deviation as the error on this value. In ten cases, however, there were not enough data in either band to perform the fit. In those cases, we set the explosion date

as the mean between the time of the last non detection and the first detection. In all but four of the cases the estimated explosion date is within less than a day from the first detection (Fig. 4; Table 2).

3.2. Peak magnitude

Following Khazov et al. (2016), we also test if events showing flash features are on average more luminous. As can be seen from Table 2, the relevant events to consider are only those with relatively early spectra. We therefore compute the peak magnitude of all seventeen events with a first spectrum obtained within 7 days from explosion. We use the forced photometry lightcurves to evaluate the peak magnitude. We fit a polynomial of order 3 to the flux measurements, over several intervals of time whose lower bound is within the first few days from

Table 3. Forced photometry of the RI sample

Object	Filter	JD	Flux [10^{-8} Mgy]	Flux error [10^{-8} Mgy]	Apparent magnitude [AB mag]	Absolute magnitude [AB mag]	Magnitude error [AB mag]
...
ZTF18aarpttw	g	2458258.8522	2.3555	0.0868	19.07	-17.60	0.04
ZTF18aatlfus	g	2458258.8564	3.9348	0.0916	18.51	-18.06	0.03
ZTF18aarqxbw	g	2458258.8624	1.4655	0.0709	19.59	-17.13	0.05
ZTF18aarqxbw	g	2458258.8634	1.4371	0.0731	19.61	-17.11	0.06
ZTF18aavpady	g	2458258.8672	1.2260	0.0633	19.78	-16.89	0.06
...

NOTE—This table includes the flux measurements returned by the forced photometry pipeline. In this table, we report the last non detections within 2.5 days from the first marshal detection and all the measurements which follow. The full version of this table is electronic.

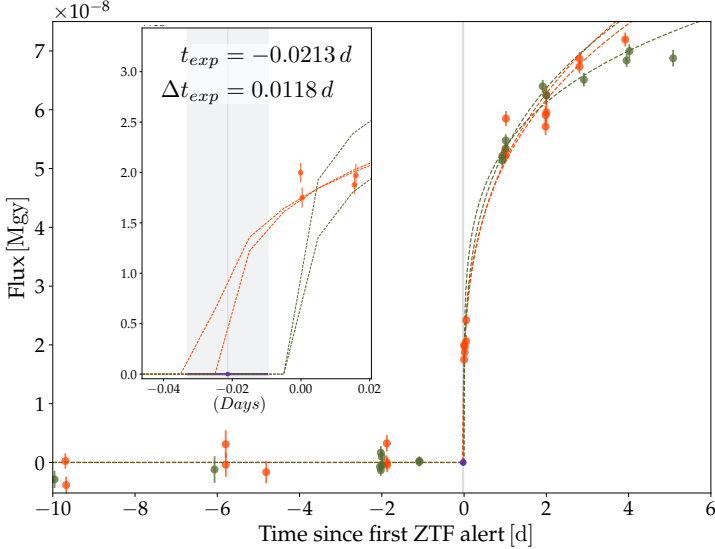


Figure 2. Early light curve fits used to determine the explosion date for SN 2018dfc. Power-law fits to the observations during the first 2 or 5 days are shown in both the g (green points) and r (red points) bands. The mean and standard deviation of the fits (inset) are adopted as the the explosion time and the error. The time origin is defined as the time of the first alert from ZTF.

explosion time and upper bound between 10 to 40 days after the estimated explosion time (Fig. 3). We adopt the mean and range of peak times obtained from these fits as the peak date and its error (vertical grey band in Fig. 3) and take the mean and standard deviation of the flux value within this range to be the peak flux and error (horizontal grey band in Fig. 3). We report these values for each event in each band in Table 4.

3.3. Early spectroscopy

We sort the 28 RI SNe in our sample according to the difference between the estimated explosion time and the time of first spectrum (Table 2, “First spectrum” column; Fig. 4). From previous work (Gal-Yam et al.

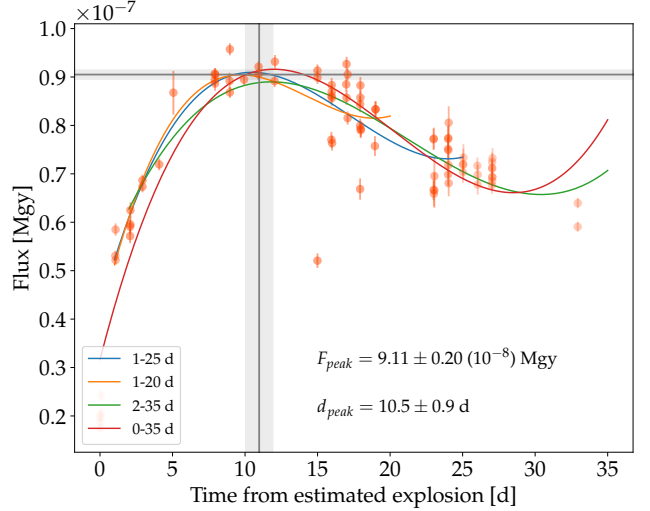


Figure 3. Example of the peak estimation in the red band for SN2018dfc. The different curves correspond to a polynomial of order 3 fitted over the time intervals noted in the legend. The cross corresponds to the peak date and flux estimated from the mean of all the values obtained, and the grey bands note the estimated errors, see text for details.

2014, Yaron et al. 2017, Khazov et al. 2016), we know that flash features are typically present from the time of explosion up to several days later. We therefore define a sub-sample including events with spectra obtained within 2 d from explosion (top of Table 2). For about one third of the total sample (ten objects) we have been able to secure a first spectrum within less than 2 days from the estimated explosion time.

Throughout the 2018 campaign, we find that seven infant supernovae of Type II show flash features (Table 2; Fig 5). Two additional infant objects were marked as potential flash events (Fig. 8; see below). Four of the seven confirmed flashers had their first spectrum obtained with SEDm.

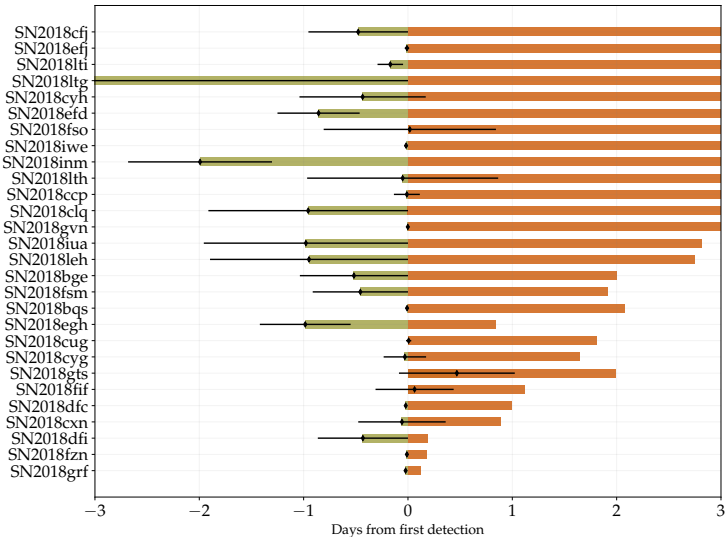


Figure 4. A graphic summary of the sample timeline, from the estimated explosion date (green) to the time of the first spectrum (red). The x-axis origin (“0” time) corresponds to the first photometric detection of each candidate. SN 2018ltg was still included in the sample of RI SNe II since its non-detection limit in the Marshal alert system was $< 2.5\text{ d}$ although the explosion time estimation with the forced photometry lightcurve puts the limits to more than three days.

The two-day sub-sample we are considering includes 6 events showing flash features (one object, SN 2018leh, shows flash features but its first spectrum was obtained only > 3 days after explosion, Table 2), the two potential flashers, and two events have high signal to noise early spectra that show no flash features (Fig. 7).

3.3.1. The Flash events

The identification of flash features in this work is solely based on the study of the spectral range surrounding the strong He II emission line at 4686 \AA . This follows previous work (Khazov et al. 2016)) and is also supported by large-scale theoretical model grids (Boian & Groh 2020) that show that this feature is ubiquitous in early spectra ($< 2\text{ d}$). We choose not to use hydrogen lines as a marker for flash features since host galaxy lines could contribute to it.

In previous well-studied cases of events with high-quality early spectra, such as SN 2013fs (Yaron et al. 2017) and SN 2013cu (Gal-Yam et al. 2014), the line He II $\lambda 4686$ is very prominent with a profile that is often well described by a narrow core with broad Lorentzian wings, which could be attributed to electron scattering within the CSM.

As discussed in detail by Soumagnac et al. (2019), as the spectra of such events evolve with time, the strong

He II emission line is replaced by a ledge-shaped feature that is probably composed of blended high-ionization lines of C, N and O. Both the He II line and the other lines are sometimes detected as a narrow emission line on top of the ledge-shaped feature (see Fig 5 and Fig. 7 of Soumagnac et al. 2019).

As several of our early spectra were obtained with the low-resolution SEDm instrument (in particular those of SN 2018grf, SN 2018gts and SN 2018cug), we can not easily differentiate between the various manifestations of the excess emission around 4686 \AA . We therefore adopt the detection of excess emission around this wavelength as our criterion for defining an object as having flash features. Analysis of the cases where we have both early SEDm spectra as well as high spectral resolution data from larger telescopes (e.g., SN 2018dfc), confirm the nature of the emission we see in the SEDm spectra and support this approach (Fig. 5).

SN 2018leh is the seventh object which displayed flash features. It does not belong to the sub-sample we are considering for this study since its first spectrum was obtained ≈ 3.7 days after the estimated explosion time. This object shows the Balmer emission lines $H\alpha$, $H\beta$, and $H\gamma$, that persist for an extended period of time, ≈ 10 days, which led us to classify this event as a SN IIn. The first spectrum also shows a strong He II line which does not show in the spectrum obtained about 10 days later, see Fig. 6. The transient He II line would technically qualify this event as a member of the flash class. A discussion of the group of objects displaying long-lived flash features and their relation to SNe IIn is outside the scope of this paper.

3.3.2. The Non-flashers

We consider an event as lacking flash features when we have early, high-quality spectra (i.e. high S/N or higher resolution than SEDm) that do not show any excess emission around He II 4686 \AA . Often, this means that the spectrum is blue and featureless. Among the ten events included in our 2-day sub-sample, SN 2018fzn was observed shortly after explosion (0.19 d, Table 2) with SEDm. While the resolution is low, the signal to noise is sufficient to determine that we cannot find any hint of possible excess emission (Fig. 7). Based on the few previous events with spectra that were obtained so early after explosion (in particular SN 2013fs; Yaron et al. 2017), we would expect strong emission lines that would be observable with SEDm (see the simulation in Extended Data Figure 2 of Gal-Yam et al. 2014). The first spectrum of SN 2018cxn was obtained with P200/DBSP less than a day past explosion. The higher resolution and the complete absence of He II emission

Table 4. Peak absolute magnitudes of the 17 objects within the 7-day spectroscopic sub-sample

IAU name	Redshift z	Distance modulus [mag]	Filter	Rise time to peak ^a [d]	Peak Flux $10^{-8}[\text{Jy}]$	Peak apparent AB mag	Peak absolute AB mag	Magnitude error
SN2018bge	0.023	35.08	g	9.9 ± 0.6	6.94 ± 0.10	17.90	-17.18	0.02
			r	18.1 ± 1.4	7.45 ± 0.05	17.82	-17.26	0.01
SN2018bqs	0.047	36.67	g	6.1 ± 0.3	3.25 ± 0.10	18.72	-17.95	0.03
			r	8.6 ± 0.7	3.20 ± 0.03	18.74	-17.93	0.01
SN2018clq	0.045	36.57	g	4.7 ± 1.2	5.93 ± 0.10	18.07	-18.51	0.02
			r	5.6 ± 1.5	5.51 ± 0.50	18.15	-18.43	0.10
SN2018cxn	0.040	36.31	g	9.8 ± 1.3	2.90 ± 0.03	18.84	-17.47	0.01
			r	15.8 ± 0.7	2.86 ± 0.02	18.86	-17.45	0.01
SN2018cug	0.050	36.81	g	8.0 ± 1.2	3.82 ± 0.06	18.54	-18.26	0.02
			r	10.3 ± 0.9	3.72 ± 0.05	18.57	-18.23	0.01
SN2018cyg	0.011	33.51	g	10.8 ± 0.6	2.14 ± 0.03	19.17	-14.33	0.02
			r	16.3 ± 0.9	5.37 ± 0.20	18.18	-15.33	0.04
SN2018dfc	0.037	36.10	g	7.5 ± 0.5	9.59 ± 0.10	17.55	-18.56	0.01
			r	10.5 ± 0.9	9.11 ± 0.20	17.60	-18.50	0.02
SN2018dfi	0.031	35.76	g	22.7 ± 0.8	3.45 ± 0.03	18.66	-17.10	0.01
			r	25.4 ± 1.1	5.64 ± 0.20	18.12	-17.64	0.04
SN2018egh	0.038	36.17	g	8.3 ± 1.7	1.61 ± 0.04	19.48	-16.69	0.03
SN2018fzn	0.037	36.16	g	19.7 ± 1.1	2.95 ± 0.03	18.83	-17.34	0.01
			r	23.1 ± 0.7	3.95 ± 0.06	18.51	-17.65	0.02
SN2018fif	0.017	34.43	g	12.2 ± 0.4	10.30 ± 0.01	17.47	-16.97	$< 10^{-2}$
			r	16.4 ± 2.7	12.80 ± 0.02	17.23	-17.20	$< 10^{-2}$
SN2018 fsm	0.040	36.30	g	6.7 ± 0.8	6.68 ± 0.06	17.94	-18.37	0.01
			r	9.5 ± 0.6	6.08 ± 0.01	18.04	-18.26	$< 10^{-2}$
SN2018gts	0.030	35.63	g	6.5 ± 0.7	2.74 ± 0.02	18.91	-16.73	0.01
			r	8.6 ± 0.6	4.76 ± 0.08	18.31	-17.33	0.02
SN2018grf	0.050	36.81	g	5.0 ± 0.1	4.40 ± 0.00	18.39	-18.41	$< 10^{-2}$
			r	7.1 ± 0.8	4.14 ± 0.03	18.46	-18.35	0.01
SN2018gvn	0.040	36.30	g	5.0 ± 0.0	4.85 ± 0.09	18.29	-18.02	0.02
SN2018iuia	0.040	36.30	g	6.4 ± 1.1	2.27 ± 0.04	19.11	-17.20	0.02
			r	15.5 ± 1.0	2.66 ± 0.00	18.94	-17.37	$< 10^{-2}$
SN2018leh	0.024	35.17	g	13.4 ± 1.0	14.70 ± 0.00	17.08	-18.08	$< 10^{-2}$
			r	17.0 ± 1.0	14.80 ± 0.03	17.07	-18.09	$< 10^{-2}$

^aFrom estimated explosion time

(Fig. 7) suggest that there were no flash features. In both cases, we conclude that there are no indications for a circumstellar shell.

3.3.3. The dubious flashers

SN 2018cyg and SN 2018egh both show excess flux around 4686 Å (Fig. 8). However, this excess does not resemble the ledge-shaped feature seen for example in the spectra of SN 2018fif (Soumagnac et al. 2019), and discussed above. An additional complication is that the spectra of SNe II at early phase (prior to the appearance of strong and broad hydrogen Balmer lines) sometime show an absorption complex extending between

$\approx 4000 - 4500 \text{ \AA}$ (E. Zimmerman et al., in preparation). Such a complex appears in the spectra of both SN 2018cyg and SN 2018egh. It is difficult to determine whether the apparent bump around 4600 Å represents an actual excess, or if it rather is the continuum edge redward of an absorption feature. In addition, even though we have secured early, high resolution spectra for these objects (Table 2) they both lack a narrow emission component from He II. These broad features are however transient and do not appear at later times. These issues makes it difficult to determine whether these events show flash features or not.

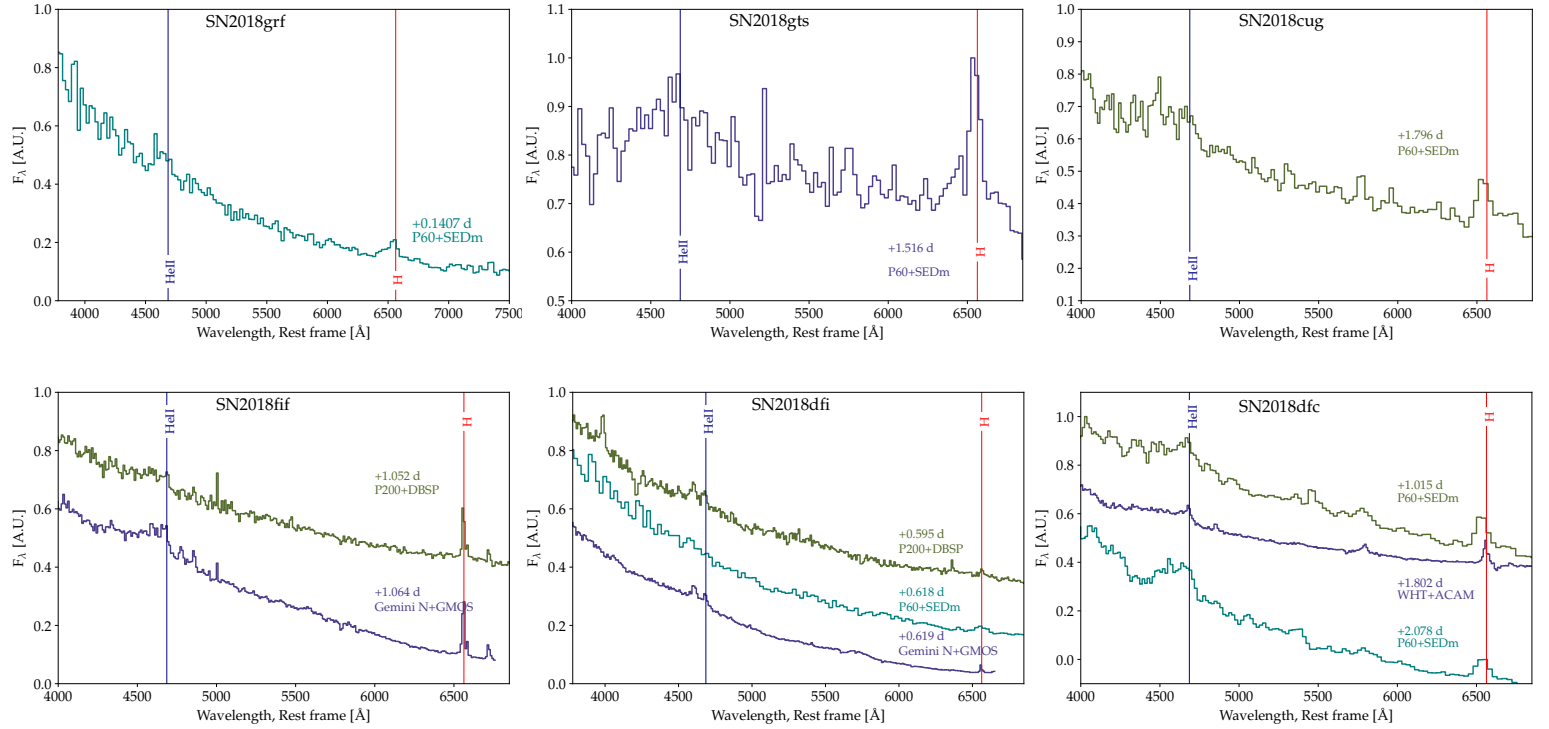


Figure 5. A collection of spectra of six confirmed Flashers. The acquisition time of the spectra are with regard to the estimated explosion date.

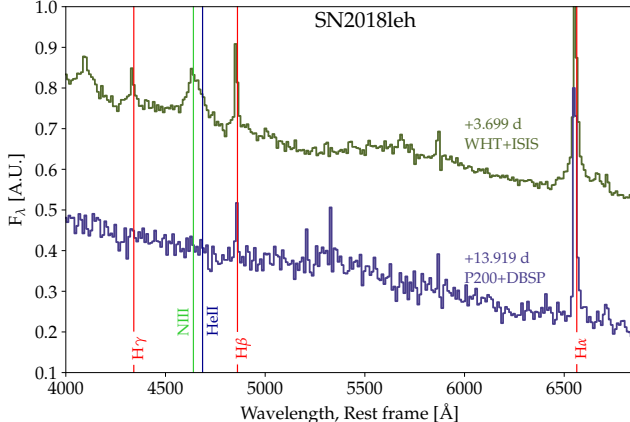


Figure 6. Spectroscopic evolution of SN 2018leh, a Type II SN that shows transient He II emission 4 days after its estimated explosion time.

As an additional test of whether these two objects show a flux excess around 4600 \AA , we conducted the following test: we constructed model spectra composed of black body continua, over which we superpose model Gaussian emission lines whose width is a free parameter (with typical best fits of $\approx 100\text{ km s}^{-1}$), in those cases (in particular, SN 2018dfc) where such lines are apparent. In addition, we add a broad feature extend-

ing between $4200 - 4750\text{ \AA}$, which we defined by fitting a third order polynomial to the ledge-shaped feature appearing in the SN 2018fif WHT spectrum (Fig. 8). The data was fitted using the python package *iminuit* (Ongmongkolkul 2012). We then performed a χ^2 test to determine whether the bump feature is significantly detected (in the sense that $\Delta\chi^2 > 1$ between models) when comparing the goodness of fit over the intervals given in Table 5.

The results of these model comparisons are reported in Table 5 and Figure 9. As can be seen, the bump is strongly detected in the spectra of SN 2018dfc (and is also recovered for SN 2018fif), but neither for SN 2018cyc nor SN 2018egh. The results do not change if we try to also fit narrow lines even to spectra where no obvious lines are seen, or if we try to fit additional weaker line features such as $H\gamma$. For SN 2018dfc, the bump feature is detected both in the earlier low-resolution SEDm spectrum (at low significance) and clearly in the later high-resolution WHT spectrum. We therefore conclude that we can not ascertain that SN 2018cyc and SN 2018egh show flash features. We conduct our analysis below and report our results for all possible options (i.e., that both, one, or neither of these show evidence for CSM).

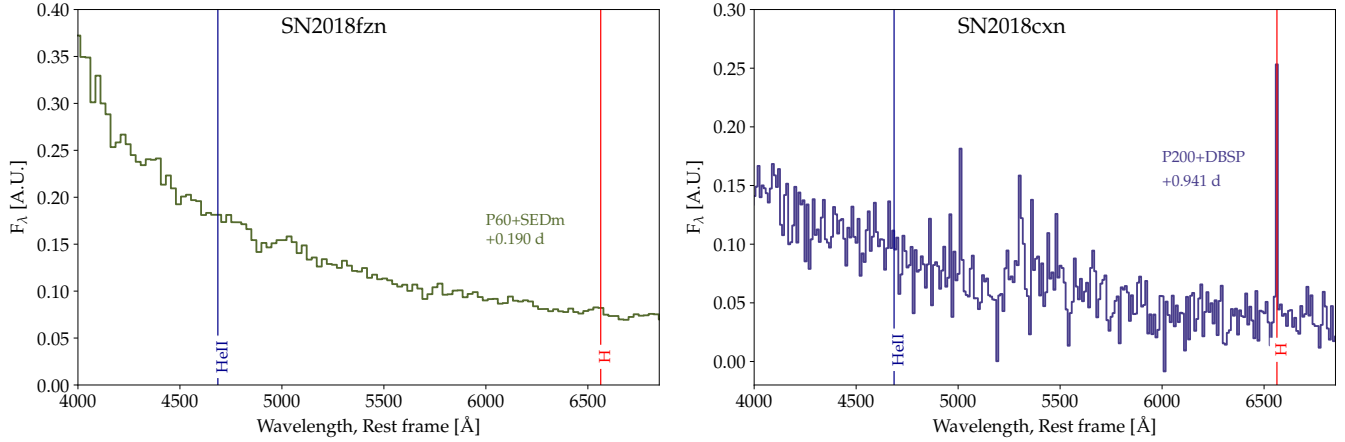


Figure 7. Early spectra of non-flashers SN 2018fzn and SN 2018cxn. These spectra were both obtained within less than a day from the estimated time of explosion. Only a smooth continuum is observed.

Table 5. Results of test fits for models with and without the broad bump feature.

Name	Spectrum	Lines fit	χ^2/dof with bump	χ^2/dof without bump	Fit Interval
SN 2018dfc	P60+SEDm +1.015 d	[HeII, H β]	0.76	1.43	4000-5300
SN 2018dfc	WHT+ACAM +1.082 d	[HeII, H β]	1.66	4.09	4000-5300
SN 2018fif	Gemini+GMOS +1.064 d	[HeII, H β]	2.12	3.34	4000-5000
SN 2018egh	WHT+ISIS +1.824 d	[HeII, H β]	0.87	0.91	4000-5300
SN 2018egh	WHT+ISIS +1.824 d	No Lines	0.87	0.93	4000-5300
SN 2018cyg	WHT+ACAM +1.673 d	No Lines	0.90	0.90	4000-5300

4. DISCUSSION AND CONCLUSIONS

4.1. How common are flash features

Based on our systematic survey of infant SNe II with spectra obtained within two days of discovery, we have found that at least 60%, and perhaps as many as 80% of the sample of ten events show evidence for flash-ionized emission. Taking into account our limited sample size and assuming binomial statistics ($\mathcal{B}(k, n, p)$), we infer the true fraction of SNe with CSM that manifests as flash features from the true probability p to observe a flash event given we the observed fraction D using a Bayesian model:

$$P(p|D) = \frac{P(D|p) \times \pi(p)}{P(D)} \quad (3)$$

Where p is the probability of observing a flash ionised event (here $p \in [0; 1]$), D is the observation presented in this paper (i.e.: 6 out of 10 candidates are showing flash features). The probability of our observation, $P(D)$ can be calculated with the formula of total probability, i.e.

$P(D) = \int_0^1 \mathcal{B}(6, 10, p) \times \pi(p) dp$. We assume a uniform distribution for the prior $\pi(p)$ which allows us to write the posterior function as:

$$P(p|D) = \frac{\binom{10}{6} p^6 (1-p)^4}{\int_0^1 \binom{10}{6} p^6 (1-p)^4 dp} \quad (4)$$

This results in a Beta distribution (see Figure 10). We can put a strict lower limit on the fraction of infant SNe II showing flash features of $> 30.8\%$ ($> 23.5\%$) at the 95% (99%) confidence level. This fraction rapidly drops when events with spectra obtained within 7 d from explosion are considered; presumably the fraction could be even higher for events with even earlier spectra.

These results are broadly consistent with previous work by Khazov et al. (2016), which estimate that 7 – 36% show flash features in spectra obtained within < 2 d from explosion (68% confidence level). It is also consistent with the low observed frequency of flash features among the general population of Type II SNe reported in the literature, as these events very rarely have

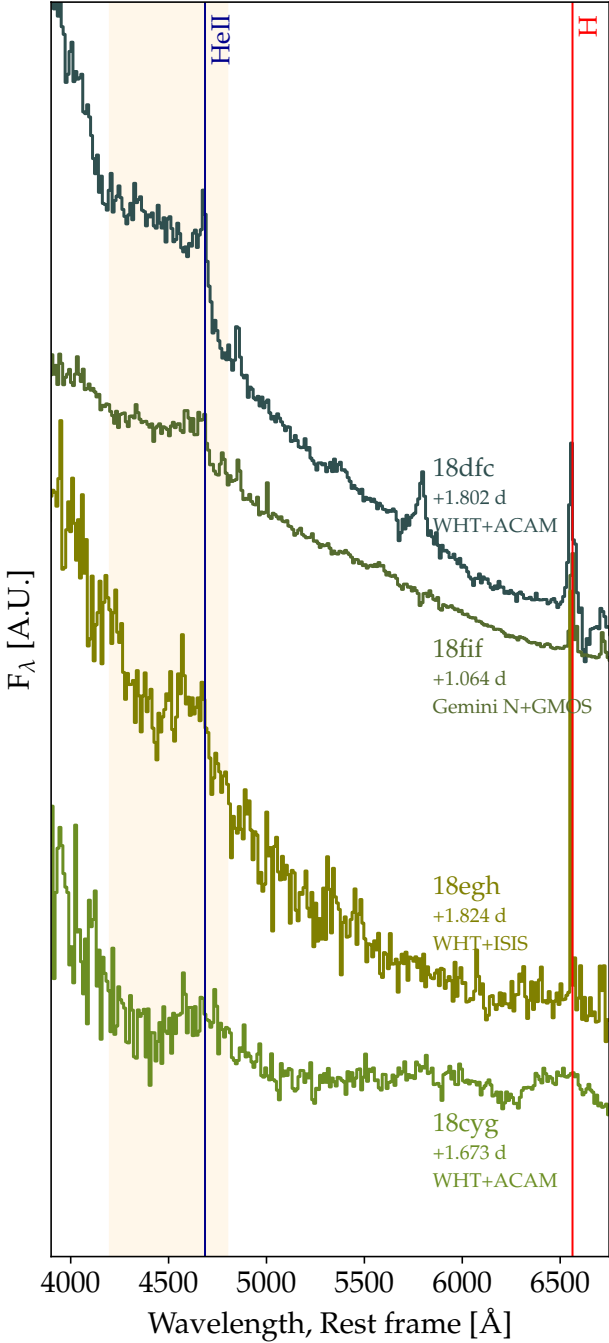


Figure 8. Candidates showing a wide bump-like structure close to the He II emission line. We highlight in orange the region we searched for excess emission.

a spectrum obtained < 2 d after explosion, and Table 2 shows that the fraction of flash events falls rapidly at ages > 2 d. The unique nightly cadence of the ZTF partnership survey enabled us to routinely discover infant SNe and rapidly obtain spectra, while the systematic design of our survey allowed for a robust measurement of the frequency of this phenomenon.

4.2. Possible biases

Khazov et al. (2016) (see their Fig. 8) show that Type II SNe showing flash-ionized features tend to be brighter at peak than other events. We cannot confirm this is also true for our sample. We consider here the subsample of Infant Supernovae whose first spectrum was obtained within less than 7 days from the estimated explosion time, the peak magnitudes were obtained following the method described in 3.3.2. Figure 11, top panel, shows the peak magnitudes in both g and r bands for flashers and non flashers. Flashers appear to be brighter in both bands. However, when one considers SN 2018cyg as a flasher, the average peak magnitude of both groups is inverted and non-flashers appear brighter than flashers (see Table 6, top section). Since SN 2018cyg is strongly reddened, we repeated this same analysis but with SN 2018cyg being host extinction corrected. To apply the extinction correction, we consider the spectrum from 2018 August, 4⁹ and apply the method described in Poznanski et al. 2012, using the line doublet of sodium. We consider the doublet not to be resolved and apply the following formula:

$$\log_{10}(E_{B-V}) = 1.17 \times EW(D_1 + D_2) - 1.85 \pm 0.08 \quad (5)$$

We estimate the EW of $D_1 + D_2$ using the built-in tool from WISeREP by measuring it several times. The mean EW is 1.64 with an error of 0.17. Following Eq. (5), the final peak magnitudes for SN 2018cyg are : $M_{peak,r} = -18.45 \pm 0.50$ and $M_{peak,g} = -18.77 \pm 0.80$. Table 6 summarises the different cases : whether SN 2018cyg is a flasher and whether SN 2018cyg was corrected for estimated host extinction. We find that flash events are not inherently brighter than non-flash events.

We also inspect in Fig. 11 (lower panel) the distribution of apparent magnitudes at discovery for our < 7 d sample. As can be seen there, we find that the flash events were not significantly brighter at discovery than other events, and thus neither more likely to be discovered, nor to be followed, as both of these depend on the apparent magnitude of the object at discovery.

4.3. Implications

We have shown here that a significant fraction, and possibly most, Type II SN progenitors, show transient emission lines in their early spectra, that provide evidence that these stars are embedded in a compact distribution of CSM (Yaron et al. 2017). The narrow width of these emission lines indicates a slow expansion speed for the CSM ($100 - 800 \text{ km s}^{-1}$, Boian & Groh 2020), and

⁹ see on WISeREP : <https://wiserep.weizmann.ac.il/object/698>

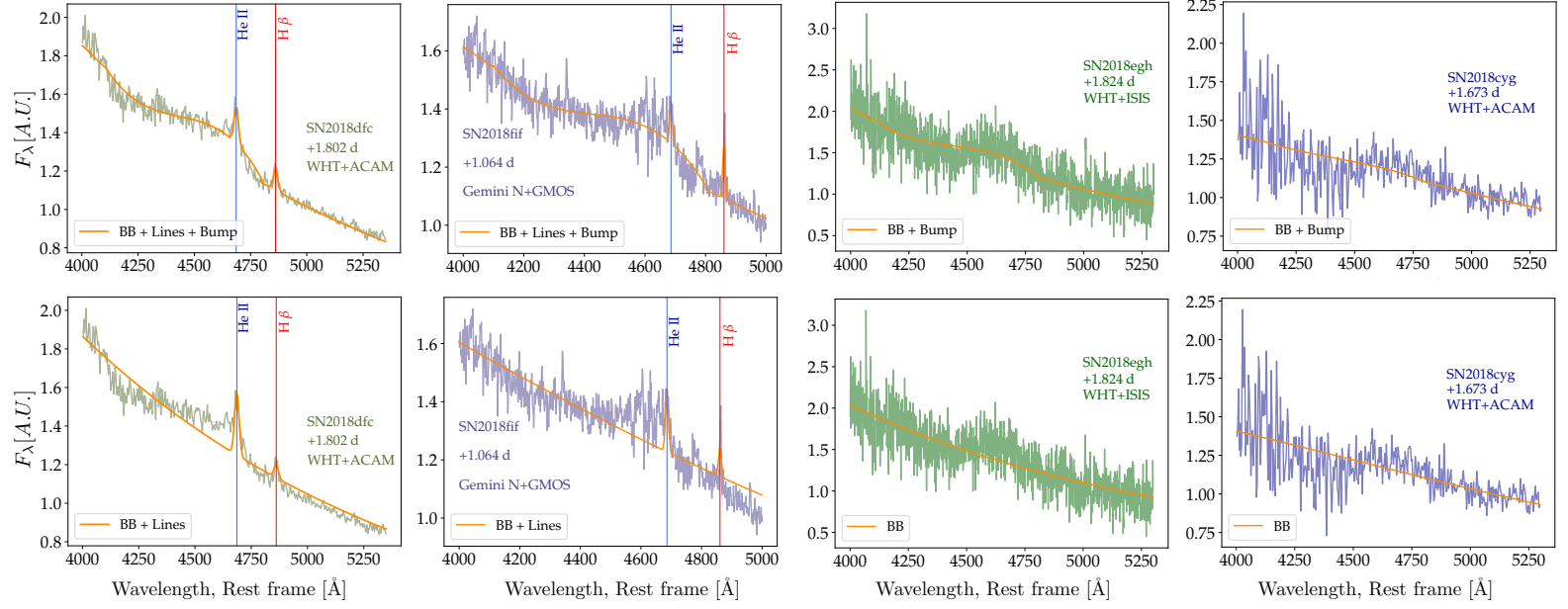


Figure 9. Fit results with (top panels) and without (bottom panels) the broad feature component for SNe 2018dfc, 2018fif, 2018egh and 2018cyg (from left to right). No narrow emission lines are seen in the spectra of 2018egh and 2018cyg, and neither provides a significant detection of a bump component.

Table 6. Peak magnitude comparison between the flash events and the non flash events.

		$M_{peak, \text{flasher}}$	$M_{peak, \text{non flasher}}$
<i>18cyg not corrected for extinction</i>			
r band	18cyg \subset flasher	-17.58 ± 0.96	-17.76 ± 0.42
	18cyg $\not\subset$ flasher	-17.91 ± 0.48	-17.46 ± 0.90
<i>18cyg corrected for extinction</i>			
	18cyg \subset flasher	-17.97 ± 0.48	-17.76 ± 0.42
	18cyg $\not\subset$ flasher	-17.91 ± 0.48	-17.85 ± 0.46
		$M_{peak, \text{flasher}}$	$M_{peak, \text{non flasher}}$
<i>18cyg not corrected for extinction</i>			
g band	18cyg \subset flasher	-17.30 ± 1.31	-17.64 ± 0.57
	18cyg $\not\subset$ flasher	-17.73 ± 0.71	-17.31 ± 1.13
<i>18cyg corrected for extinction</i>			
	18cyg \subset flasher	-17.86 ± 0.75	-17.64 ± 0.57
	18cyg $\not\subset$ flasher	-17.76 ± 0.75	-17.75 ± 0.64

NOTE— This analysis is performed with the subsample which has a first spectrum within less than seven days from the estimated explosion time.

combined with its compact radial dimension ($< 10^{15}$ cm) we have evidence that the CSM was deposited by the stars within months to a few years prior to its terminal explosion. Assuming these progenitors are mostly red supergiants (RSGs; Smartt 2015), this would suggest that most exploding RSGs experience an enhanced mass loss shortly prior to explosion.

While RSGs certainly lose mass during their final stages of evolution (Smith 2014), such a period of enhanced mass loss shortly (months to a year) prior to explosion is not explained by standard stellar evolution models. Our work thus may indicate that additional physical processes leading to such pre-explosion instabilities (e.g., Arnett & Meakin 2011, Shiode & Quataert

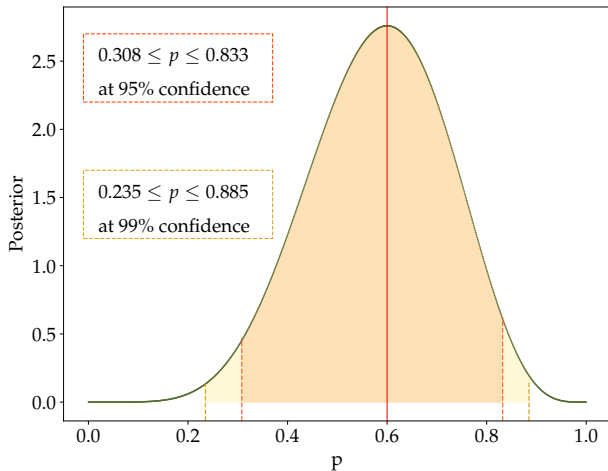


Figure 10. Posterior probability distribution vs. the probability to observe a flash ionised event. This analysis is based on the subsample of infant candidates which had a first spectrum within < 2 days from the estimated explosion date. The lower limit is 30.8% (23.5%) at 95%(99%) confidence interval.

2014) not only exist, but are ubiquitous among massive stars.

As we have shown that most SN II progenitors likely undergo a remarkable evolution shortly prior to explosion, it may be needed to re-examine the stellar models used as initial conditions to explosion simulations. In particular, at least some of the effects proposed to explain such pre-explosion mass loss, may render the spherical pre-explosion stellar models used in explosion simulations less realistic (Arnett & Meakin 2016). Perhaps our work thus provides a clue how to tackle some of the problems encountered in trying to reproduce the observed distribution of SN explosions using numerical explosion models.

5. CONCLUSIONS

We report the results from the first year (2018) of our systematic survey for infant Type II SNe in the ZTF partnership survey. We collected 28 such objects (at a rate of about one per week) and obtained rapid follow-up spectroscopy within 2 d from explosion for 10 events. Between 6 – 8 of these show evidence for transient emission from a surrounding distribution of CSM, and we can thus place a strict lower limit of $> 30\%$ (at 95% C.L.) on the fraction of SN II progenitors that explode within compact CSM distributions. This finding is inconsistent with predictions from standard stellar evolution models, and suggests that additional physics is required to explain the final stages (~ 1 year prior to explosion) of massive star evolution. The structural changes that may

accompany such final episodes of intense mass loss can modify the stellar structure prior to explosion and may require adjusting the initial conditions assumed for core-collapse SN explosion simulations, and may thus shed light on the yet unsolved question of how massive stars end their life in supernova explosions.

6. ACKNOWLEDGEMENTS

AGY's research is supported by the EU via ERC grant No. 725161, the ISF GW excellence center, an IMOS space infrastructure grant and BSF/Transformative and GIF grants, as well as The Benoziyo Endowment Fund for the Advancement of Science, the Deloro Institute for Advanced Research in Space and Optics, The Veronika A. Rabl Physics Discretionary Fund, Paul and Tina Gardner, Yeda-Sela and the WIS-CIT joint research grant; AGY is the recipient of the Helen and Martin Kimmel Award for Innovative Investigation. The ztfquery code was funded by the European Research Council (ERC) under the European Union's Horizon 2020 research and innovation programme (grant agreement No. 759194 - USNAC, PI: Rigault). The ZTF forced-photometry service was funded under the Heising-Simons Foundation grant #12540303 (PI: Graham). Based on observations obtained with the Samuel Oschin 48-inch Telescope at the Palomar Observatory as part of the Zwicky Transient Facility project. ZTF is supported by the National Science Foundation under Grant No. AST-1440341 and a collaboration including Caltech, IPAC, the Weizmann Institute for Science, the Oskar Klein Center at Stockholm University, the University of Maryland, the University of Washington, Deutsches Elektronen-Synchrotron and Humboldt University, Los Alamos National Laboratories, the TANGO Consortium of Taiwan, the University of Wisconsin at Milwaukee, and Lawrence Berkeley National Laboratories. Operations are conducted by COO, IPAC, and UW. The data presented here were obtained [in part] with ALFOSC, which is provided by the Instituto de Astrofísica de Andalucía (IAA) under a joint agreement with the University of Copenhagen and NOTSA. A.A.M. is funded by the LSST Corporation, the Brinson Foundation, and the Moore Foundation in support of the LSSTC Data Science Fellowship Program; he also receives support as a CIERA Fellow by the CIERA Postdoctoral Fellowship Program (Center for Interdisciplinary Exploration and Research in Astrophysics, Northwestern University).

7. APPENDIX

The full list of candidate infant SNe II returned by `ztfquery` (see § 2.2) is given in Table 7. Of the 43

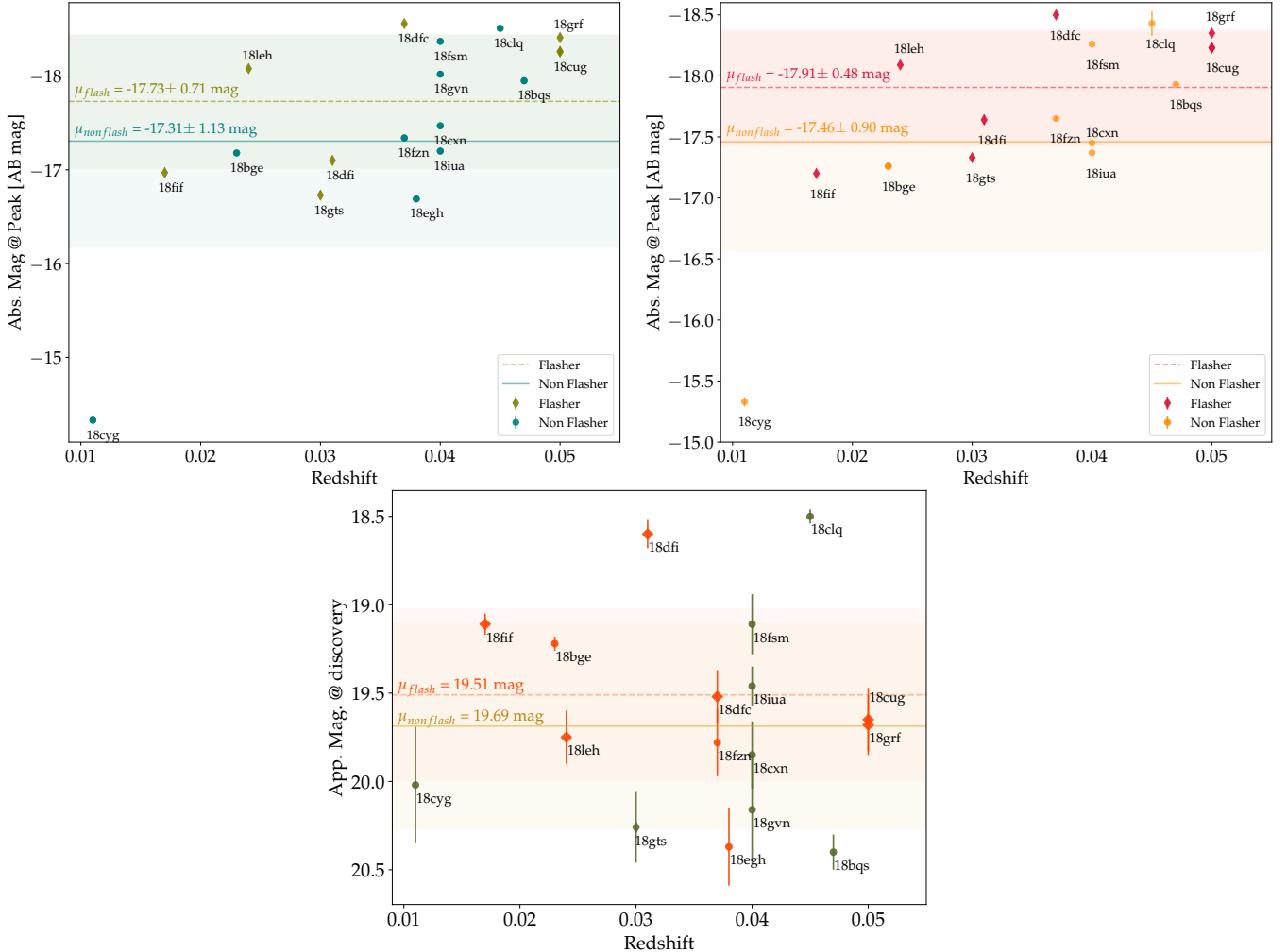


Figure 11. Top: absolute magnitude in r band (left) and g band (right) vs. redshift. Bottom: apparent magnitude at discovery vs. redshift. Color bands represent the error on the mean peak magnitude for both flash and non flash groups. SN 18cyg is host reddened and hence appears very faint, see text.

candidates, inspection shows that 15 are spurious, and these have been removed from our sample. We provide some comments on removed objects.

Early false positives—A group of objects detected right at the start of the survey (during March 2018 till early April) suffered from unreliable photometry, manifest as a mix of detections and non-detections during the same period, and often during the same night. This is likely due to problematic early references. The mix of detections and non-detections created artificial triggers due to a spurious non-detection just prior to the first detection. This group includes ZTF18aaayemw, ZTF18aaccmnh, ZTF18aagrded (which was also detected by ATLAS 3 days prior to the ZTF false non-detection, and reported to the TNS as AT2018ahi), ZTF18aahrzrb, ZTF18aainvic, and ZTF18aaogibq.

ZTF18aaqkdwu—This trigger resulted from a spurious photometry point generated by the pipeline at the location of SN 2019eoe a year prior to the explosion of the actual SN.

ZTF18aasxvsg—Additional analysis recovered several clear detections prior to the spurious non-detection that triggered this event.

ZTF18abcqhg—This event is likely a real infant SN II, but we could not recover it using the forced photometry pipeline and it was therefore removed from the sample. This object does not have an early spectrum.

ZTF18acbuvwsp—This event was detected by SNHunt and reported to the TNS as AT 2018hqm a few days prior to the only ZTF non-detection, indicating it is likely not a RI SN.

ZTF18acecuxq—The early photometry of this event shows a mix of detections and non-detections during the same nights, and was deemed unreliable. A spectrum obtained within a day of the false non-detection (A. Tzanidakis, in preparation) is that of an old SN II, supporting this conclusion.

ZTF18acvgviq—This event was detected by ATLAS and reported to the TNS as SN 2018fru more than 2 months prior to the ZTF non-detection, indicating our non-detections preceding the ZTF first detection were spurious.

ZTF18acefuhk—Updated photometry does not recover a non-detection prior to first detection that satisfies our criteria. This object does not have early spectra.

ZTF18acqxyiq—The forced photometry pipeline did not recover the non-detection by the real-time pipeline, leaving the explosion time poorly constrained.

ZTF18adbikdz—This object was detected by Gaia and reported to the TNS as AT2017isr over a month prior to the first detection by ZTF (when it was already declining). Our single non-detection is spurious.

REFERENCES

- Arnett, W. D., & Meakin, C. 2011, ApJ, 733, 78
- . 2016, Reports on Progress in Physics, 79, 102901
- Astropy Collaboration, Robitaille, T. P., Tollerud, E. J., et al. 2013, A&A, 558, A33
- Bellm, E. C., & Sesar, B. 2016, pyraf-dbsp: Reduction pipeline for the Palomar Double Beam Spectrograph, , , ascl:1602.002
- Bellm, E. C., Kulkarni, S. R., Graham, M. J., et al. 2019, PASP, 131, 018002
- Ben-Ami, S., Konidaris, N., Quimby, R., et al. 2012, in Society of Photo-Optical Instrumentation Engineers (SPIE) Conference Series, Vol. 8446, Proc. SPIE, 844686
- Benn, C., Dee, K., & Agócs, T. 2008, in Society of Photo-Optical Instrumentation Engineers (SPIE) Conference Series, Vol. 7014, Proc. SPIE, 70146X
- Blagorodnova, N., Neill, J. D., Walters, R., et al. 2018, PASP, 130, 035003
- Boian, I., & Groh, J. H. 2020, MNRAS, 496, 1325
- Bruch, R. 2020, Transient Name Server Classification Report, 2020-1575, 1
- Cardelli, J. A., Clayton, G. C., & Mathis, J. S. 1989, ApJ, 345, 245
- Cenko, S. B., Fox, D. B., Moon, D.-S., et al. 2006, PASP, 118, 1396
- Davenport. 2018, pyDIS, vdoi, , , doi:doi:10.5281/zenodo.58753. <https://github.com/TheAstroFactory/pydis>
- Dessart, L., John Hillier, D., & Audit, E. 2017, A&A, 605, A83
- Drake, A. J., Gänsicke, B. T., Djorgovski, S. G., et al. 2014, MNRAS, 441, 1186
- Dugas, A., Fremling, C., & Sharma, Y. 2019, Transient Name Server Classification Report, 2019-1402, 1
- Filippenko, A. V. 1997, ARA&A, 35, 309
- Foley, R. J., Smith, N., Ganeshalingam, M., et al. 2007, ApJL, 657, L105
- Fremling, C., Dugas, A., & Sharma, Y. 2018a, Transient Name Server Classification Report, 2018-1519, 1
- . 2018b, Transient Name Server Classification Report, 2018-1567, 1
- . 2018c, Transient Name Server Classification Report, 2018-1444, 1
- . 2018d, Transient Name Server Classification Report, 2018-1597, 1
- . 2018e, Transient Name Server Classification Report, 2018-1828, 1
- . 2018f, Transient Name Server Classification Report, 2018-1340, 1
- . 2019, Transient Name Server Classification Report, 2019-826, 1
- Fremling, C., & Sharma, Y. 2018a, Transient Name Server Classification Report, 2018-1028, 1
- . 2018b, Transient Name Server Classification Report, 2018-1034, 1
- . 2018c, Transient Name Server Classification Report, 2018-939, 1
- . 2018d, Transient Name Server Classification Report, 2018-904, 1
- Fremling, C., Sharma, Y., & Dugas, A. 2018g, Transient Name Server Classification Report, 2018-1404, 1
- . 2018h, Transient Name Server Classification Report, 2018-1071, 1
- . 2018i, Transient Name Server Classification Report, 2018-1349, 1
- . 2018j, Transient Name Server Classification Report, 2018-1108, 1
- Gaia Collaboration, Brown, A. G. A., Vallenari, A., et al. 2018, A&A, 616, A1
- Gal-Yam, A. 2017, Observational and Physical Classification of Supernovae, ed. A. W. Alsabti & P. Murdin, 195

- Gal-Yam, A. 2019, in American Astronomical Society Meeting Abstracts, Vol. 233, American Astronomical Society Meeting Abstracts #233, 131.06
- Gal-Yam, A., Schulze, S., Soumagnac, M., & Yaron, O. 2018, Transient Name Server Classification Report, 2018-1237, 1
- Gal-Yam, A., Kasliwal, M. M., Arcavi, I., et al. 2011, ApJ, 736, 159
- Gal-Yam, A., Arcavi, I., Ofek, E. O., et al. 2014, Nature, 509, 471
- Garnavich, P. M., & Ann, H. B. 1994, AJ, 108, 1002
- Gehrels, N., Chincarini, G., Giommi, P., et al. 2004, ApJ, 611, 1005
- Graham, M. J., Kulkarni, S. R., Bellm, E. C., et al. 2019, PASP, 131, 078001
- Groh, J. H. 2014, A&A, 572, L11
- Hiramatsu, D., Arcavi, I., Burke, J., et al. 2018, Transient Name Server Classification Report, 2018-974, 1
- Hook, I. M., Jørgensen, I., Allington-Smith, J. R., et al. 2004, PASP, 116, 425
- Hosseinzadeh, G., Valenti, S., Arcavi, I., et al. 2015, in American Astronomical Society Meeting Abstracts, Vol. 225, American Astronomical Society Meeting Abstracts #225, 140.08
- Hosseinzadeh, G., Valenti, S., McCully, C., et al. 2018, ApJ, 861, 63
- Karamehmetoglu, E., Fransson, C., Sollerman, J., et al. 2019, arXiv e-prints, arXiv:1910.06016
- Kasliwal, M. M., Cannella, C., Bagdasaryan, A., et al. 2019, PASP, 131, 038003
- Khazov, D., Yaron, O., Gal-Yam, A., et al. 2016, ApJ, 818, 3
- Kiewe, M., Gal-Yam, A., Arcavi, I., et al. 2012, ApJ, 744, 10
- Law, N. M., Kulkarni, S. R., Dekany, R. G., et al. 2009, PASP, 121, 1395
- Masci, F. J., Laher, R. R., Rusholme, B., et al. 2019, PASP, 131, 018003
- Moriya, T. J., Yoon, S.-C., Gräfener, G., & Blinnikov, S. I. 2017, MNRAS, 469, L108
- Neill, J. D. 2019, in The Extragalactic Explosive Universe: the New Era of Transient Surveys and Data-Driven Discovery, 38
- Niemela, V. S., Ruiz, M. T., & Phillips, M. M. 1985, ApJ, 289, 52
- Nyholm, A., Sollerman, J., Tartaglia, L., et al. 2019, arXiv e-prints, arXiv:1906.05812
- Ofek, E. O., Sullivan, M., Shaviv, N. J., et al. 2014, ApJ, 789, 104
- Oke, J. B., & Gunn, J. E. 1982, PASP, 94, 586
- Oke, J. B., Cohen, J. G., Carr, M., et al. 1995, PASP, 107, 375
- Ongmongkolkul, P. 2012, iminuit, a Jupyter-friendly Python frontend to the MINUIT2 C++ library, vdoi, Zenodo, doi:10.5281/zenodo.3949207. <https://doi.org/10.5281/zenodo.3949207>
- Pastorello, A., Smartt, S. J., Mattila, S., et al. 2007, Nature, 447, 829
- Pastorello, A., Wang, X. F., Ciabattari, F., et al. 2016, MNRAS, 456, 853
- Patterson, M. T., Bellm, E. C., Rusholme, B., et al. 2018, Publications of the Astronomical Society of the Pacific, 131, 018001. <http://dx.doi.org/10.1088/1538-3873/aae904>
- Perley, D. A. 2019, PASP, 131, 084503
- Poznanski, D., Prochaska, J. X., & Bloom, J. S. 2012, Monthly Notices of the Royal Astronomical Society, 426, 14651474. <http://dx.doi.org/10.1111/j.1365-2966.2012.21796.x>
- Prentice, S. 2018, Transient Name Server Classification Report, 2018-630, 1
- Quimby, R. M., Wheeler, J. C., Höflich, P., et al. 2007, ApJ, 666, 1093
- Rigault, M. 2018, ztfquery, a python tool to access ZTF data, vdoi, Zenodo, doi:10.5281/zenodo.1345222. <https://doi.org/10.5281/zenodo.1345222>
- Rigault, M., Neill, J. D., Blagorodnova, N., et al. 2019, A&A, 627, A115
- Schlafly, E. F., & Finkbeiner, D. P. 2011, ApJ, 737, 103
- Schlegel, E. M. 1990, MNRAS, 244, 269
- Shiode, J. H., & Quataert, E. 2014, ApJ, 780, 96
- Smartt, S. J. 2015, PASA, 32, e016
- Smith, N. 2014, ARA&A, 52, 487
- Soumagnac, M. T., Ganot, N., Gal-Yam, A., et al. 2019, arXiv e-prints, arXiv:1907.11252
- Taddia, F., Stritzinger, M. D., Sollerman, J., et al. 2013, A&A, 555, A10
- Wright, E. L., Eisenhardt, P. R. M., Mainzer, A. K., et al. 2010, AJ, 140, 1868
- Yaron, O., & Gal-Yam, A. 2012, PASP, 124, 668
- Yaron, O., Gal-Yam, A., Ofek, E., & Sass, A. 2019, Transient Name Server AstroNote, 37, 1
- Yaron, O., Perley, D. A., Gal-Yam, A., et al. 2017, Nature Physics, 13, 510
- Zackay, B., Ofek, E. O., & Gal-Yam, A. 2016, ApJ, 830, 27

Table 7. Results of the search for infant SN II using ZTFquery

Name	RA [deg]	Dec [deg]	Redshift	First Detection [days]	First spectrum [days]	Real?
ZTF18aaayemw	134.8982936	45.6116267	0.052	2458156.7621	0.024	✗
ZTF18aaccmnh	194.9769678	37.8589965	0.0356	2458184.8604	0.018	✗
ZTF18aagrded	209.8414748	46.0317554	0.047	2458198.8809	0.011	✗
ZTF18aahrzrb	181.397224	34.3888035	0.04	2458217.7371	1.001	✗
ZTF18aainvic	256.5204624	29.6683607	0.03175	2458218.9088	0.019	✗
ZTF18aaogibq	253.5409858	24.721127	0.037	2458231.8783	0.020	✗
ZTF18aaqkdwu	199.7588529	45.0263019	0.06037	2458243.677	0.001	✗
ZTF18aaqkoyr	166.0666639	50.0306275	0.023	2458243.6854	1.036	✓
ZTF18aarpttw	247.2599041	43.6268239	0.047	2458246.822	1.001	✓
ZTF18aarqxbw	276.4265403	34.6584885	0.048	2458246.8404	1.878	✓
ZTF18aasxvsg	217.1290246	37.0678367	0.0248	2458244.8361	0.018	✗
ZTF18aatlfus	257.1764284	28.5206128	0.0451	2458249.8534	1.913	✓
ZTF18aavpady	273.0031098	44.3602114	0.047	2458257.8452	0.870	✓
ZTF18aawyjjq	263.0587448	36.0740074	0.04	2458263.796	0.011	✓
ZTF18aayxxew	197.1395703	45.9861525	0.061	2458278.7043	1.961	✓
ZTF18abcezmh	269.4519011	40.0764001	0.057	2458288.7881	0.874	✓
ZTF18abckutn	237.0269066	55.7148077	0.0401	2458290.6992	0.834	✓
ZTF18abcptmt	267.3298968	49.4124315	0.05	2458291.7869	0.878	✓
ZTF18abcqhgr	254.818188	60.4317998	0.070396	2458291.8048	0.021	✗
ZTF18abdbysy	233.5352962	56.6968517	0.01127	2458295.7208	0.016	✓
ZTF18abddjpt	278.7048393	38.2987246	0.07	2458295.7913	0.021	✓
ZTF18abeajml	252.0323502	24.3041089	0.03651	2458303.7989	1.002	✓
ZTF18abffyqp	252.7086818	45.397907	0.031302	2458307.6862	0.864	✓
ZTF18abgqvww	254.3164613	31.9632993	0.0377	2458313.7295	0.891	✓
ZTF18abgrbjb	274.9986631	51.7965471	0.03	2458313.7492	0.032	✓
ZTF18abimhf	240.1422651	31.6429838	0.05	2458320.6667	0.912	✓
ZTF18abojpnr	297.4871203	59.5928266	0.0375	2458351.7166	0.021	✓
ZTF18abokyfk	2.3606444	47.3540929	0.017189	2458351.8659	0.887	✓
ZTF18abrljlc	253.1840255	70.0882366	0.05	2458359.7	0.054	✓
ZTF18absldfl	33.5997507	30.811929	0.04	2458363.8793	0.913	✓
ZTF18abufaej	4.4825733	12.0916007	0.0625	2458368.8738	0.036	✓
ZTF18abvvmdf	249.1975409	55.7358424	0.029597	2458375.7154	0.016	✓
ZTF18abwlsoi	261.8976711	71.5302584	0.05	2458377.6334	0.895	✓
ZTF18abyvenk	273.9764532	44.6964862	0.04	2458385.6212	0.858	✓
ZTF18acbvwsp	341.9067649	39.8806077	0.017062	2458423.6368	0.907	✗
ZTF18acecuxq	68.8323442	17.1948085	0.02572	2458431.8168	1.011	✗
ZTF18acefuhk	136.7936282	43.9207446	0.057	2458426.9469	0.951	✗
ZTF18acvgviq	204.0157722	66.3012068	0.01055	2458432.0181	1.966	✗
ZTF18achtnvk	96.1687142	46.5039037	0.04	2458434.9036	0.043	✓
ZTF18acploez	130.03737	68.9031912	0.04	2458440.9658	1.957	✓
ZTF18acqxyiq	149.8258285	34.895493	0.03849	2458443.9437	0.001	✗
ZTF18adbikdz	252.014493	26.2118328	0.03432	2458482.0504	0.004	✗
ZTF18adbmrug	61.2637352	25.2619198	0.02396	2458482.6991	1.897	✓

NOTE—43 candidates were found, of which 15 ($\sim 35\%$) were spurious, leaving 28 infant SNe II in our sample